The Connectivity of Millimeter-Wave Networks in Urban Environments Modeled Using Random Lattices

Kaifeng Han, Kaibin Huang, Ying Cui and Yueping Wu

arXiv:1702.03372v1 [cs.IT] 11 Feb 2017

Abstract

Millimeter-wave (mmWave) communication opens up tens of *giga-hertz* (GHz) spectrum in the mmWave band for use by next-generation wireless systems, thereby solving the problem of spectrum scarcity. Maintaining connectivity stands out to be a key design challenge for mmWave networks deployed in urban regions due to the blockage effect characterising mmWave propagation. Specifically, mmWave signals can be blocked by buildings and other large urban objects. In this paper, we set out to investigate the blockage effect on the connectivity of mmWave networks in a Manhattan-type urban region modeled using a random regular lattice while *base stations* (BSs) are Poisson distributed in the plane. In particular, we analyse the connectivity probability that a typical user is within the transmission range of a BS and connected by a line-of-sight. Using random lattice and stochastic geometry theories, different lower bounds on the connectivity probability are derived as functions of the buildings' size and probability of a lattice cell being occupied by a building as well as BS density and transmission range. The asymptotic connectivity probability is also derived for cases of dense buildings. Last, the results are extended to heterogeneous networks. Our study yields closed-form relations between the parameters of the building process and the BS process, providing useful guidelines for practical mmWave network deployment.

Index Terms

Millimeter-wave networks, radio access networks, network connectivity, random lattice, stochastic geometry, wireless propagation.

K. Han and K. Huang are with the Dept. of EEE at The University of Hong Kong, Hong Kong. Y. Cui is with the Department of EE, Shanghai Jiao Tong University, Shanghai 200240, China. Y. Wu is with Hong Kong Applied Science and Technology Research Institute (ASTRI), Hong Kong. Corresponding email: huangkb@eee.hku.hk.

I. Introduction

Exploiting the tens-of-GHz of available bandwidth in the *millimeter-wave* (mmWave) band is embraced by both the industry and academia as a key solution for spectrum scarcity faced by 5G in view of the exponential traffic growth [1]. Consequently, mmWave communications are expected to play a key role in delivering extreme broadband access to ultra-dense mobile users in next-generation systems [2]. Though the physics of mmWave propagation are not yet fully understood, measurement results show that the main characteristic of a mmWave channel is that signals are blocked (or at least severely attenuated) by objects in an urban environment (e.g., buildings), known as the *blockage effect*, which is much less severe in the microwave band below 6-GHz [3], [4]. In next-generation cellular networks, dense small-cell *base stations* (BSs) will be deployed at flexible locations in-between or inside buildings, unlike macro-cell BSs installed typically on rooftops [2]. Then to operate the networks in the mmWave band, maintaining reliable connectivity for mobile users appears to be a key design challenge due to the blockage effect. Therefore, from the perspective of implementing mmWave radio access networks, referred to simply as mmWave networks in this paper, it is important to quantify network connectivity based on a reasonable propagation model for the urban environment. To this end, we adopt the classic Manhattan-type urban model where the spatial distributions of buildings follow a random regular lattice and the stochastic geometry network model where BSs are randomly deployed following a *Poisson point process* (PPP) for the case of a single-tier network or K-tier PPPs for the case of *heterogeneous network* (HetNet). The level of connectivity in a mmWave network is measured using the metric of *connectivity probability*, defined as the probability that a typical mobile has a *line-of-sight* (LoS) link with at least one BS within a given transmission range. Then based on the said model, the connectivity probability is analyzed as a function of the building density as well as other network parameters.

A. Modeling Propagation in Millimeter-Wave Networks

Theoretic studies of traditional cellular networks are commonly based on the abstracted probabilistic channel models, e.g., Rayleigh or Rician fading, which were proposed based on rich scattering resulting from reflection and refraction properties for propagation with frequencies far below those of mmWaves [5]. Such models are unsuitable for mmWave propagation where due to the said blockage effect, channels are dominated by LoS links [6]. Consequently, to study the performance of mmWave networks, it is necessary to adopt propagation models that reflect

the geometry and layout of blockage and scatter objects in the environment. Several well-known relevant modeling approaches are described as follows.

1) Measurement Based Models: Perhaps the most accurate approach for studying mmWave propagation is *ray tracing* that traces signal paths by simulation using a measurement based model accounting for geometric properties of objects in the propagation environment (e.g., locations, sizes, heights and orientations of buildings) or even their physical characteristics (e.g., surface materials) as well as atmospherical conditions [7], [8]. Though being a powerful tool for practical system design, simulation based ray tracing techniques do not yield mathematical tractability due to their high complexity and hence find little use in performance analysis of mmWave networks. For such studies, the propagation models constructed using probability or stochastic geometry theories find their strengths as described shortly.

A simple measurement based model that can account for building blockage in mmWave propagation is one from the *3GPP standard* where a random link belongs to either of the LoS or non-LoS types with given probabilities [9]. The LoS and non-LoS probabilities can be fitted to a specific site by measurement, e.g., the New York city [10], [11]. The distribution was found to be frequency independent for all bands up to 100 GHz [12], making the model mmWave compatible. Though being simple, the binary channel-type model is too coarse for depicting the detailed building layout needed for studying large-scale networks.

2) Stochastic Geometry Models: Recently, modeling an urban region using stochastic geometry (e.g., Boolean model or Poisson line process) has emerged to be a promising approach for analyzing and designing large-scale mmWave networks for two main reasons [13], [14]. First, stochastic geometry provides a sufficiently elaborate and reasonable description of the random spatial distribution of blockage objects, accounting for their densities and geometric properties (e.g., shapes, orientations and sizes). Second, such an urban model can be superimposed with a classic stochastic geometry network model to yield a tractable model for a mmWave network. The application of stochastic geometry to model and design wireless networks is a well-established approach (see e.g., the survey in [15]). Specifically, the spatial distribution of network nodes can be represented by a suitable choice from a wide range of spatial point processes such as Poisson spatial tessellations for cellular networks [16] or cluster point processes for ad hoc radios [17]. The superposition of stochastic geometry models for blockage objects and network nodes (BSs and mobiles) in an urban region allows the application of stochastic geometry theory to quantify the effects of blockage on the performance of mmWave networks.

There exist two main stochastic geometry urban models used in the performance analysis

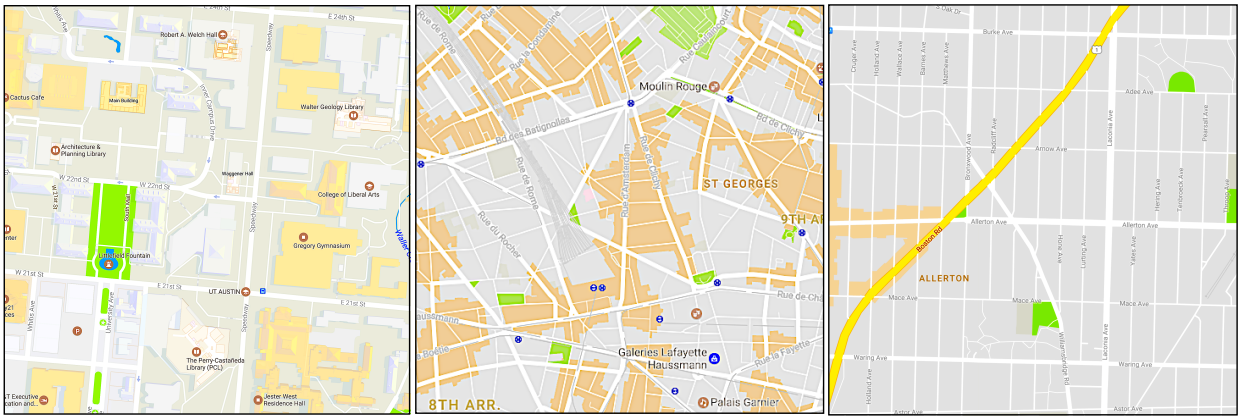

(a) University of Texas at Austin, USA (b) Paris, France (c) Manhattan, New York, USA

Figure 1: Examples of urban regions: (a) University of Texas at Austin, USA, (b) Paris, France and (c) Manhattan, New York, USA that can be approximated using the random-shape, Poisson-line and random-lattice models, respectively.

of mmWave networks. The first one is the *Boolean model* considered in [13] where blockage objects are rectangular distributed in a plane following the Boolean model and having random sizes and orientations. The model is suitable for the type of urban regions similar to the campus of The University of Texas at Austin, USA as shown in Fig. 1(a), characterized by random and irregular blockage distributions. Combining the model and a network model with Poisson distributed BSs, random shape theory and other stochastic-geometry tools are applied for characterising the mmWave-network coverage by analysing the signal-and-interference distributions. For tractable analysis, it is assumed in [13] that different channels are independent of each other. The assumption does not hold in practice since an object with large volume can block multiple mmWave links simultaneously with nonzero probability, introducing *correlated blockage* for nearby links. Most recently, the blockage spatial correlation is studied in [18] using the Boolean model where buildings are represented by random line segments, and furthermore how blockage affects the networks reliability is characterised, with the consideration of users' macro diversity gain.

The second urban model, namely *Poisson-line model*, is applied in [14] for studying wireless networks with shadowing (or blockage) in an urban environment, where the distribution of streets in the urban region can be represented by a Poisson-line process. Such a model is suitable for cities with randomly oriented streets such as Paris, France as illustrated in Fig. 1(b). In the mmWave-network model building on the said urban model, network nodes located on and off the lines are considered as being outdoor and indoor, respectively. Two outdoor locations along the same line are connected by a LoS or otherwise by a non-LoS (with blockage), thereby accounting

for correlated blockage. Based on the model, the spatial correlation of channel shadowing is analysed, providing results for studying the interference distribution and network coverage [14].

In addition, there exists a simplified model, called *LoS-ball model*, for blockage effect as developed in [19], [20] for use in stochastic geometry network models. In the blockage model, a link between a BS-mobile pair is assumed to have a LoS only if the separation distance is shorter then a given threshold. Compared with the random-shape and Poisson-line models, the current one substantially simplifies the network-performance analysis but at the cost of losing an elaborate geometric description of blockage objects.

3) Random-Lattice Models: The urban regions in some cities are suitably modeled using random (square) lattices but not the previously discussed random-shape or Poisson-line processes. One example is Manhattan, New York, USA as illustrated in Fig. 1(c), giving the random-lattice urban models the well-known name of Manhattan-type models. In such models, each square cell of the lattice is occupied by an object (e.g., a building) with a given probability and the locations of different cells are *independent and identically distributed* (i.i.d.). In the area of wave propagation, the models have been widely used for representing scatterers in an urban region and used to analyze the distributions of wave-propagation distances in a given direction for a fixed number of reflections [21]–[23]. However, the applications of random-lattice urban models in network modeling remain an area being largely explored, as the approach usually fails to yield tractable network-performance analysis.

B. Analysing Network Connectivity

The connectivity of spatially random ad hoc networks is a classic research area (see e.g., [15], [24], [25]). Two radio nodes are connected if they are within each other's transmission ranges. Then an ad hoc network is connected if all nodes for a single connected cluster with a probability close to one [26]. In a fully connected ad hoc network, any pair of nodes can communicate via multi-hop transmissions. Network connectivity typically exhibits a phase-transition phenomenon where the network is fully connected almost surely if a particular network parameter, e.g., node transmission power [27] or interference density [28], satisfies some requirements. Different network models and analytical approaches have been proposed for studying network connectivity such as stochastic-geometric model and theory [29] or random matrix theory [30].

Due to the severe blockage effect, maintaining connectivity has appeared to be a key challenge for designing next-generation mmWave networks, which is an area largely uncharted and motivates the current work. A classic network model for studying connectivity essentially consists

of a set of randomly distributed nodes. In contrary, we consider mmWave radio access networks and propose a more complex stochastic geometry model comprising buildings (blockage objects) distributed as a random lattice and multi-tier BSs distributed as independent PPPs. Moreover, the connectivity for the mmWave networks is defined such that a typical user is connected to the network if the user lies within the transmission range of at least one BS and they are connected by a LoS. The definition differs from the mentioned classic one for ad hoc networks.

C. Our Contributions

The models and network performance metric for this work are elaborated as follows. The mmWave network is assumed to be deployed in a Manhattan-type urban region. As mentioned, the existing spatial blockage models, including the Boolean model [13] and the Poisson-line model [14], are unsuitable. Thus the buildings are modeled using a random regular lattice, which partitions the plane into square sites for measuring the building size. The buildings are overlaid with Poisson distributed BSs. We consider both single-tier and multi-tier BSs, modeled as a single PPP and multiple independent PPPs, respectively. The analysis focuses on a typical outdoor user at the origin while the extension of the results to a randomly located user is discussed. Then the network performance is measured by the *connectivity probability* and defined as the probability that the typical user is within the transmission range of at least one BS and furthermore they are connected by a LoS (unblocked by buildings). Interference is omitted in the analysis for simplicity, which can be justified by the fact that blockage and sharp beamforming enabled by mmWave jointly suppress interference and cause mmWave networks to usually operate in the noise-limited regime [2]. One can see that the connectivity probability depends on both the distributions of the buildings and BSs. By jointly applying the theories of random lattice and stochastic geometry, bounds on the connectivity probability are derived in closed form.

The main contributions of the current work are summarised as follows.

1) First, we consider a single-tier network. Define the blockage-free region as the region around the typical outdoor user that is free of buildings. A closed-form lower bound on the connectivity probability can be derived by inner bounding the blockage-free region by a disk centered at the user with a random radius. Using the bound and Poisson distribution of BSs, the lower bound on the connectivity probability is derived as a function of building parameters (e.g., size and site-occupancy probability) and BS parameters (e.g., transmission range and BS density). For dense sites, an asymptotic lower bound on the connectivity probability is derived, which has a simple form than the non-asymptotic counterpart.

Table I: Summary of Notation

Notation	Meaning
s	Area of site
λ_s	The density of sites
$(a\sqrt{s}, b\sqrt{s})$, $\mathcal{S}_{a,b}$	The coordinate of site, the (a,b)th site
Φ, $\tilde{\Phi}$	The random lattice process of a uniform-height blockage model, a K-height blockage model
p_b, $p_b^{(k)}$	Site occupation probability in a uniform-height blockage model, a K-height blockage model
Σ, $\Sigma^{(k)}$	The random region covered by buildings in a uniform-height blockage model, a K-height blockage model
Π, λ_c	The PPP modeling BSs in the single-tier network, its density
$\Pi^{(k)}$, $\lambda_c^{(k)}$	The PPP modeling BSs in the kth tier network, its density
r_b, $r_b^{(k)}$	Radius of BS's coverage region in the single-tier, the kth tier network
Y_n	Location of BS
U_0	Central located typical user
$\mathcal{F}$, $\mathcal{F}^{(k)}$	Blockage-free region of typical user a uniform-height blockage model, a K-height blockage model
$\mathcal{B}$	Disk region
$N(\cdot)$	Number of sites (either fully or partially) covered by a disk $\mathcal{B}$
p_c, $p_c^{(k)}$, $\widehat{p}_c$	Connectivity probability for the single-tier, the kth tier network, the K-tier HetNet

2) Next, the preceding lower bounds for the single-tier network are tightened by finding a tighter inner bound of the said blockage-free region. The technique is to partition the region into multiple sub-regions and inner bound each by a sector. The union of the sectors gives the said tighter inner bound on the blockage-free region. Then tighter bounds of connectivity probability are derived.
3) Last, the preceding results are extended to a K-tier HetNet, comprising K-tier BSs with varying transmission ranges and densities over the tiers. Buildings with varying heights are also considered. The building with random height blocks the signals transmitted by a corresponding subset of BS tiers. It is shown that the connectivity probability of the K-tier HetNet increases linearly with the number of tiers.

The remainder of the paper is organized as follows. The models and performance metric are described in Section II. The network connectivity are analysed for a single-tier network and a K-tier HetNet in Section III and Section IV, respectively. Simulation results are presented in Section V followed by concluding remarks in Section VI.

II. Models and Metric

The models and network performance metric are described in the following sub-sections. The notation is summarised in Table I.

A. Blockage Spatial Distribution

We model the mmWave blockage objects, namely buildings, in a Manhattan-type urban region using a random lattice process defined as follows. As illustrated in Fig. 2, consider a regular lattice with density λ_s that partitions the plane into uniform square areas of size $s = \frac{1}{\lambda_s}$, each called a site. For ease of expression, the center of each site is referred to as a lattice point. Let an arbitrary lattice point be the origin of plane $\mathbb{R}^2$. Then the lattice points can be written as the set $\{(a\sqrt{s}, b\sqrt{s})|(a,b) \in \mathbb{Z}^2\}$ and the (a,b)th site as $\mathcal{S}_{a,b}$, where $\mathbb{Z}$ denotes the set of integers.

First, consider a uniform-height blockage model. That is, building heights are uniform. The random lattice, denoted as Φ, represents a set of i.i.d. Bernoulli random variables $\Phi = \{\mathcal{Z}_{a,b} \in \{0,1\}|(a,b) \in \mathbb{Z}^2\}$, where $\mathcal{Z}_{a,b} = 1$ and 0 with probabilities p_b and $\bar{p}_b = (1 - p_b)$, respectively. Here, $\mathcal{Z}_{a,b} = 1$ indicates that the site $\mathcal{S}_{a,b}$ is occupied by a building, and $\mathcal{Z}_{a,b} = 0$ otherwise. The random region of plane $\mathbb{R}^2$ covered by buildings is the union of the regions of the sites in $\{(a,b) \in \mathbb{Z}^2|\mathcal{Z}_{a,b} = 1\}$, represented by Σ.

The above model can be extended to a K-height blockage model with densities varying for buildings with different random heights. This model is more practical, as buildings in an urban region usually have different densities and heights. The K different building heights are denoted by $h^{(k)},\ k = 1, \cdots, K$. Suppose $h^{(1)} > \cdots > h^{(K)} > 0$. For ease of notation, set $h^{(0)} = 0$. The effect of building heights on blockage is reflected in that buildings of heights $h^{(1)}, \cdots, h^{(k)}$ can block signals transmitted by the kth tier BSs, which is illustrated in the sequel. The random lattice of the K-height blockage model, denoted as $\tilde{\Phi}$, represents a set of i.i.d. random variables $\tilde{\Phi} = \{\mathcal{Z}_{a,b} \in \{h^{(0)}, h^{(1)}, \cdots, h^{(K)}\}|(a,b) \in \mathbb{Z}^2\}$, where $h^{(k)}$ with probabilities $p_b^{(k)}$. Here, $\mathcal{Z}_{a,b} = h^{(0)} = 0$ indicates that the site $\mathcal{S}_{a,b}$ is not occupied by a building, and $\mathcal{Z}_{a,b} = h^{(k)} > 0$ indicates that it is occupied by a building of height $h^{(k)}$, where $k = 1, \cdots, K$. In addition, the probabilities $p_b^{(0)}$ and $p_b^{(k)}$ determine the density of empty sites and that of buildings of height $h^{(k)}$, where $k = 1, \cdots, K$. The random building region corresponding to buildings of height $h^{(k)}$ is the union of the regions of the sites in $\{(a,b) \in \mathbb{Z}^2|\mathcal{Z}_{a,b} = h^{(k)}\}$, represented by $\Sigma^{(k)}$, where $k = 1, \cdots, K$. Note that $\{\Sigma^{(k)}\}$ are correlated.

B. Network Spatial Distribution

First, consider a single-tier network comprising homogeneous BSs as shown in Fig. 2(a). The BS locations are modeled as a homogeneous PPP $\Pi = \{Y_n\}$ with density λ_c, where $Y_n \in \mathbb{R}^2$ corresponds to the location of a particular BS. The BSs (or users) located in occupied sites can be treated as the *indoor* BSs (or users) while others as the *outdoor* BSs (or users). For simplicity,

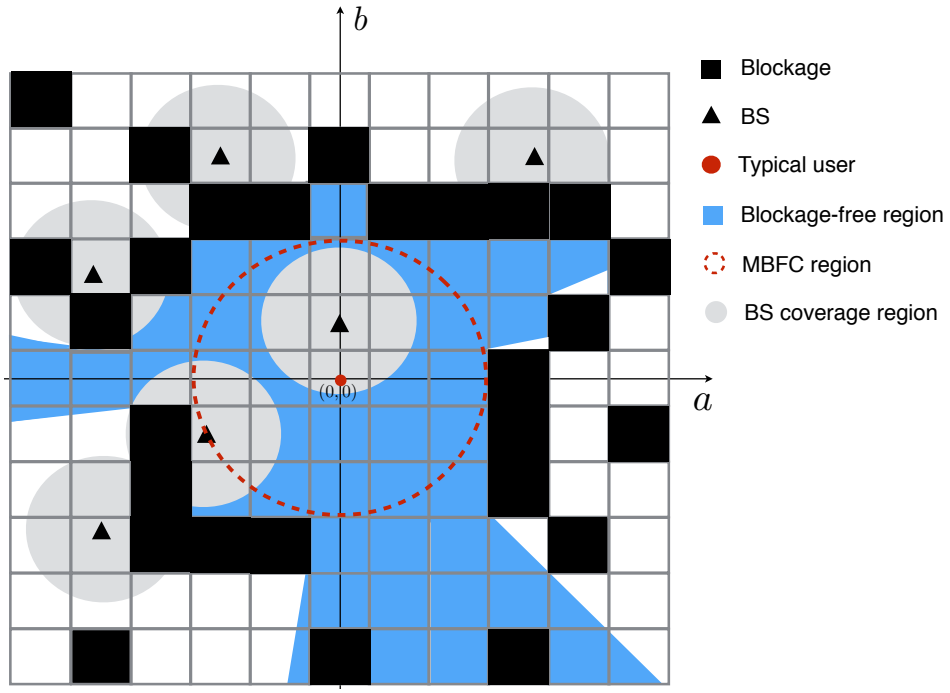

(a) Single-tier Network

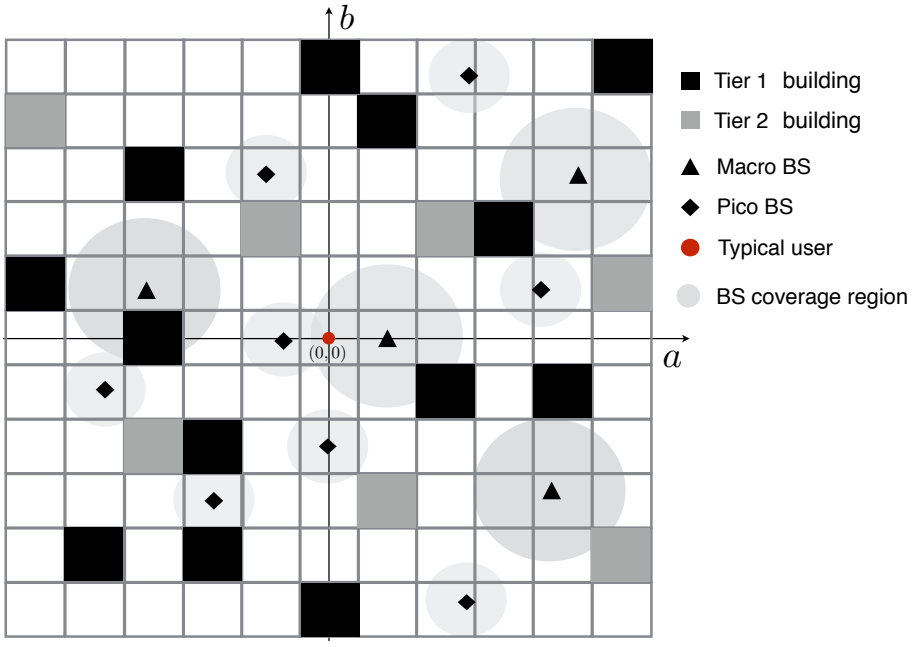

(b) Two-tier Network

Figure 2: The spatial distribution of buildings, BSs, typical user in mmWave networks.

the network performance analysis focuses on a typical outdoor user, denoted by U_0, located at the origin and the extension of the analysis to a randomly located user is subsequently discussed.

Next, consider a HetNet comprising K tiers of BSs as shown in Fig. 2(b). The spatially distribution of BSs in the kth tier follows a homogeneous PPP with density $\lambda_c^{(k)}$, denoted as

$\Pi^{(k)}$, where $k = 1, \cdots, K$. Suppose $\lambda_c^{(1)} < \lambda_c^{(2)} < \cdots < \lambda_c^{(K)}$. The PPPs $\{\Pi^{(k)}\}$ are independent. All BSs in the same tier have the same transmission power. Suppose the tier with a small index has a higher transmission power, namely the 1st tier BSs have the largest transmission power while BSs in the Kth tier have the smallest one. The BSs with a higher transmit power have a larger transmission range (e.g., macro BSs) and are overlaid by different classes of denser yet smaller coverage BSs (e.g., pico BSs or femto BSs). We consider the open-access strategy where any mobile user is allowed to connect to any BS tier without any restriction.

C. Channel Model

Following [9], the channel between a BS and a user is of either LoS or non-LoS, depending on whether it is intercepted by a building. For the case of non-LoS, the complete blockage of signals is assumed for simplification, reflecting severe propagation loss from penetrating or scattering by buildings [6], [13]. On the other hand, for the case of LoS, the channel is assumed to have path-loss but no small-scale fading. As mentioned, interference is assumed to be suppressed by sharp beamforming at BSs using large-scale arrays and also blockage by buildings. For a user to connect to a BS, two conditions have to be satisfied. First, given fixed BS transmission power and required receive SNR, the separation distance between the user and the BS is shorter than a constant, called the *coverage (service) range* of the BS. Second, there has to be a LoS channel between them. A user is connected to the network if it connects to at least one BS.

D. Performance Metric

Consider the single-tier network. The network performance is measured by the metric of connectivity probability p_c defined as the probability that the typical user U_0 is connected to the network. Recall that the typical user U_0 is connected to the single-tier network if it is in the service range of at least one BS such that the BS is linked with U_0 by a LoS. Mathematically, the connectivity probability can be defined as follows. Let $\mathcal{B}(r_b)$ denote the disk centered at U_0 and with the radius r_b, where r_b represents the coverage range of a BS in the single-tier network. Let $L(A, B) \triangleq \{cA + (1-c)B | A \in \mathbb{R}^2, B \in \mathbb{R}^2, 0 \leq c \leq 1\}$ denote the line segment connecting two points $A \in \mathbb{R}^2$ and $B \in \mathbb{R}^2$ in the plane. For the typical user U_0, define the random *blockage-free region* in the single-tier network as all points in the plane that are connected to U_0 by LoS, denoted by $\mathcal{F} \triangleq \{X \in \mathbb{R}^2 | L(X, U_0) \cap \Sigma = \emptyset\}$. Then, for the single-tier network, the connectivity probability p_c can be written as

$$p_c = \Pr\{\mathcal{F} \cap \mathcal{B}(r_b) \cap \Pi \neq \emptyset\}. \tag{1}$$

Note that $\mathcal{F}$ and Π depend on the blockage and BS distributions, respectively.

Consider the K-tier HetNet. Let $r_b^{(k)}$ represent the coverage radius of BSs in the kth tier. Recalling the assumption that the tier with a smaller index has a higher transmission power, we have $r_b^{(1)} > r_b^{(2)} > \cdots > r_b^{(K)}$. Recall that signals from a BS in the kth tier can be blocked by buildings of heights $h^{(1)}, \cdots, h^{(k)}$. Similar to the single-tier network scenario, the random blockage-free region for the kth tier is given by $\mathcal{F}^{(k)} = \{X \in \mathbb{R}^2 | L(X, U_0) \cap (\cup_{\ell=1}^{k} \Sigma^{(\ell)}) = \emptyset\}$. Therefore, the connectivity probability for the kth tier network is

$$p_c^{(k)} = \Pr\left\{\mathcal{F}^{(k)} \cap \mathcal{B}(r_b^{(k)}) \cap \Pi^{(k)} \neq \emptyset\right\}. \tag{2}$$

Moreover, recalling the used open-access strategy, the event that the typical user covered by the K-tier HetNet is equivalent to that the set $\bigcup_{k=1}^{K}\left(\mathcal{F}^{(k)} \cap \mathcal{B}(r_b^{(k)}) \cap \Pi^{(k)}\right)$ is not empty. Then, for the K-tier HetNet, the connectivity probability $\widehat{p}_c$ can be written as

$$\widehat{p}_c = \Pr\left\{\bigcup_{k=1}^{K}\left(\mathcal{F}^{(k)} \cap \mathcal{B}(r_b^{(k)}) \cap \Pi^{(k)}\right) \neq \emptyset\right\}. \tag{3}$$

Note that $\mathcal{F}^{(k)}$ and $\Pi^{(k)}$ depend on the distributions of buildings of heights $h^{(1)}, \cdots, h^{(k)}$ and the distribution of BSs in the kth tier, respectively.

III. Connectivity of Single-tier Network

It is challenging to derive the network connectivity probability due to the irregularity of the proposed blockage-free region. In this section, we derive its lower bounds with simple and insightful forms for the two cases of normal and high site densities by applying random-lattice and stochastic-geometry theories.

A. Bounding Connectivity Probabilities

1) Normal Site Density: Consider the case in which the site density λ_s is normal. The case is equivalent to one where each site has a normal areas. For this case with finite λ_s, considering a typical outdoor mobile located at the origin for simplicity, a lower bound on the connectivity probability p_c defined in (1) is derived in this subsection.

First of all, some useful results are derived as follows.

Lemma 1. Given $r > 0$, the number of sites (either fully or partially) covered by the disk $\mathcal{B}(r)$, denoted as $N(r)$, is given as follows.

– For a small ratio $\frac{r}{\sqrt{s}}$, $N(r)$ satisfies $N^-(r) \le N(r) \le N^+(r)$ with

$$N^-(r) = \left(2\left\lceil \frac{r}{\sqrt{2s}} - \frac{1}{2}\right\rceil^+ + 1\right)^2, N^+(r) = \left(2\left\lceil \frac{r}{\sqrt{s}} - \frac{1}{2}\right\rceil^+ + 1\right)^2, \tag{4}$$

where the operator $\lceil x \rceil^+ = \max(\lceil x \rceil, 0)$.

– For a large ratio $\frac{r}{\sqrt{s}} \gg 1$, $N(r)$ is given by

$$N(r) = \frac{\pi r^2}{s} + O\left(\frac{r}{\sqrt{s}}\right). \tag{5}$$

Note that the lower and upper bounds on $N(r)$ given in (4) are derived by calculating the largest number of sites fully covered by $\mathcal{B}(r)$ and the smallest number of sites fully covering $\mathcal{B}(r)$, respectively (see Fig. 2(a)). In addition, the value of $N(r)$ in (5) is obtained by ignoring boundary effects and focusing on the ratio between the area of $\mathcal{B}(r)$ and that of a site only.

Next, to derive a simple and insightful lower bound on p_c, we introduce the *maximum (inscribed) blockage-free circular* (MBFC) region. Specifically, let

$$\begin{aligned} R \triangleq \arg\max \quad & r \\ \mathbf{s.t.} \quad & r \in \left\{ \sqrt{s}(n+\frac{1}{2}) \middle| n = 0, 1, \cdots \right\}, \\ & \mathcal{B}(r) \cap \Sigma = \emptyset. \end{aligned} \tag{6}$$

Note that $R \in \{\sqrt{s}(n+\frac{1}{2}) | n = 0, 1, \cdots\}$ is a discrete random variable with the randomness included by the blockage region Σ. The discreteness of R is due to that of Σ. The MBFC region is centered at the origin with radius R, denoted by $\mathcal{B}(R)$. The distribution of R is given as follows.

Lemma 2 (Distribution of R)**.** The *probability mass function* (PMF) of R is given by[1]

$$\Pr(R = r_n) = \bar{p}_b^{4(n+\frac{1}{2})^2 - 1} - \bar{p}_b^{4(n+\frac{3}{2})^2 - 1}, \qquad n = 0, 1, 2, \cdots, \tag{7}$$

where $r_n \triangleq \sqrt{s}(n+\frac{1}{2})$.

Proof: See Appendix A. □

Using the above results, the connectivity probability p_c can be lower bounded as follows. One can see that the MBFC region inner bounds the blockage-free region for the considered typical mobile: $\mathcal{B}(R) \subseteq \mathcal{F}$. Then replacing $\mathcal{F}$ with $\mathcal{B}(R)$ in the definition of p_c in (1) gives:

$$p_c \ge \Pr\Big\{ \mathcal{B}(R) \cap \mathcal{B}(r_b) \cap \Pi \ne \emptyset \Big\}$$

[1]Note that $N(r_n) = 4(n+\frac{1}{2})^2 - 1$.

$$= \Pr\Big\{\mathcal{B}\Big(\min(R, r_b)\Big) \cap \Pi \neq \emptyset\Big\} \tag{8}$$

$$= \mathsf{E}\Big[1 - e^{-\pi\lambda_c(\min(R,r_b))^2}\Big]$$

$$= \left(1 - e^{-\pi\lambda_c r_b^2}\right) \Pr\left(R \geq r_b\right) + \sum_{n=0}^{\lfloor \frac{r_b}{\sqrt{s}} - \frac{1}{2} \rfloor^+} \left(1 - e^{-\pi\lambda_c r_n^2}\right) \Pr(R = r_n), \tag{9}$$

where the operator $\lfloor x \rfloor^+ = \max(\lfloor x \rfloor, 0)$. Note that the two terms in (9) correspond to the cases of $R \geq r_b$ and $R < r_b$, respectively. In particular, in the case of $R < r_b$, R takes the values in $\{r_n | r_n < r_b\}$. On the other hand, leveraging the result in Lemma 1, we have

$$\begin{aligned} \Pr\left(R \geq r_b\right) &= \left(1 - p_b\right)^{N(r_b)-1} \\ &\geq \left(1 - p_b\right)^{N^+(r_b)-1}. \end{aligned} \tag{10}$$

Substituting the distribution of R in Lemma 2 and (10) into (9) gives the following main result of this sub-section.

Theorem 1 (Connectivity Probability for the Single-tier Network)**.** The connectivity probability for the single-tier network can be lower bounded as follows:

$$p_c \geq \Big(1 - e^{-\pi\lambda_c r_b^2}\Big)\bar{p}_b^{N^+(r_b)-1} + \sum_{n=0}^{\lfloor \frac{r_b}{\sqrt{s}} - \frac{1}{2} \rfloor^+} \Big(1 - e^{-\pi\lambda_c s(n+\frac{1}{2})^2}\Big)\bar{p}_b^{4(n+\frac{1}{2})^2-1}\Big(1 - \bar{p}_b^{8(n+1)}\Big), \tag{11}$$

where $N^+(r_b)$ is given in (4).

For the lower bound on p_c in Theorem 1, the two terms correspond to the cases of $R \geq r_b$ and $R < r_b$, respectively. Note that $r_b > r_n$ for $n = 0, 1, \cdots, \lfloor \frac{r_b}{\sqrt{s}} - \frac{1}{2} \rfloor^+$ implying $N^+(r_b) > N(r_n) = 4(n + \frac{1}{2})^2 - 1$. Thus, the first term is dominant if the buildings are sparse, i.e., p_b is small (or $\bar{p}_b$ is large), and the second term is dominant if the buildings are dense, i.e., p_b is large (or $\bar{p}_b$ is small). Next, one can observe from the result that the key parameters that determine the connectivity probability are the site-void probability $\bar{p}_b$, the BS density λ_c and the coverage radius r_b. To be specific, p_c is a monotone-increasing function of the two BS parameters (λ_c and r_b) and also $\bar{p}_b$ when $\bar{p}_b$ is small. In particular, p_c approaches one exponentially fast as λ_c grows.

2) High Site Density: Consider the case of dense sites ($\lambda_s \to \infty$). In this case, the discreteness of the blockage region Σ varnishes such that the radius of the MBFC region, R, can be approximated as a continuous random variable with the following distribution:

$$\Pr(R \geq r) = \bar{p}_b^{\lambda_s \pi r^2 + O(\sqrt{\lambda_s r^2})}, \qquad \lambda_s \to \infty, \tag{12}$$

based on Lemma 1. It follows the lower bound on p_c in (9) can be written as:

$$p_c \geq \left(1-e^{-\pi\lambda_c r_b^2}\right)\bar{p}_b^{\pi\lambda_s r_b^2} + 2\pi\int_0^{r_b}\left(1-e^{-\pi\lambda_c r^2}\right)\lambda_s \ln\frac{1}{\bar{p}_b}\bar{p}_b^{\lambda_s\pi r^2} r\mathrm{d}r, \qquad \lambda_s\to\infty,$$
$$= \frac{\lambda_c}{\lambda_c-\lambda_s\ln\bar{p}_b}\left(1-\bar{p}_b^{\lambda_s\pi r_b^2}e^{-\pi\lambda_c r_b^2}\right) + \frac{\lambda_s\ln\bar{p}_b}{\lambda_s\ln\bar{p}_b-\lambda_c}\left(1-e^{-\pi\frac{\lambda_c}{\lambda_s}}\right). \tag{13}$$

Applying the result given in (13) yields the following main result of the sub-section.

Theorem 2 (Connectivity Probability for the Single-tier Network with a High Site Density)**.** For the case of dense sites ($\lambda_s\to\infty$), the connectivity probability for the single-tier network is lower bounded as follows:

$$p_c \geq \frac{1}{1+\frac{\lambda_s}{\lambda_c}\ln\frac{1}{\bar{p}_b}}\left(1-e^{-\lambda_c\pi r_b^2(1+\frac{\lambda_s}{\lambda_c}\ln\frac{1}{\bar{p}_b})}\right) + \frac{1}{1+\frac{\lambda_c}{\lambda_s\ln\frac{1}{\bar{p}_b}}}\left(1-e^{-\pi\frac{\lambda_c}{\lambda_s}}\right). \tag{14}$$

Theorem 2 provides a closed-form lower bound on the connectivity probability for the single-tier network with dense sites. One can be observed from the result in (14) is that for given BS density λ_c, the lower bound on p_c decreases to zero as the building density λ_s grows to infinity due to the blockage effect. On the other hand, the effect can be counteracted by increasing the BS density λ_c, as the lower bound on p_c depends on the ratio between λ_c and λ_s for the high building density case. The rule of thumb on the required density can be obtained from (14) as follows. Assuming that the site occupation probability p_b is small, we have

$$\ln\frac{1}{\bar{p}_b} = \ln\frac{1}{1-p_b} \approx p_b. \tag{15}$$

Substituting (15) into (14) yields

$$p_c \geq \frac{1}{1+\frac{\lambda_s p_b}{\lambda_c}}\left(1-e^{-\lambda_c\pi r_b^2(1+\frac{\lambda_s p_b}{\lambda_c})}\right) + \frac{1}{1+\frac{\lambda_c}{\lambda_s p_b}}\left(1-e^{-\pi\frac{\lambda_c}{\lambda_s}}\right). \tag{16}$$

Then a required value of p_c can be guaranteed if the ratio $\frac{\lambda_s p_b}{\lambda_c}$ is fixed, for small p_b.

B. Tightening the Bounds on Connectivity Probabilities

In this section, we derive lower bounds on the connectivity probability under normal and high site densities that are tighter than those in the preceding sub-section. The key idea is to define an inner bound of the blockage-free region $\mathcal{F}$ that is tighter than the MBFC region $\mathcal{B}(R)$ defined in preceding sub-section. One promising way is to partition the plane into multiple non-overlapping regions and define corresponding non-overlapping blockage-free regions, whose union yields the desired inner bound of $\mathcal{F}$. Given the typical outdoor mobile at the origin, we consider one particular partition of $\mathbb{R}^2\backslash\mathcal{S}_{0,0}$ that comprises eight non-overlapping regions (with an entire site

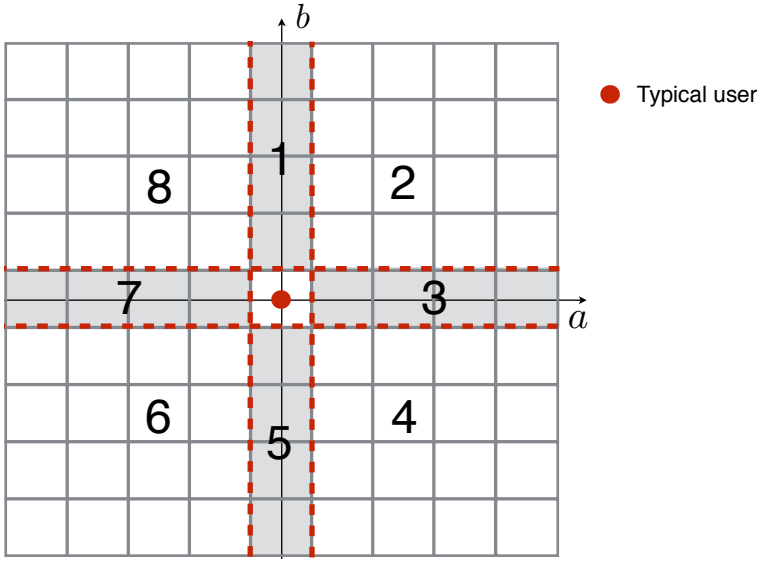

Figure 3: Dividing the urban region into eight non-overlapping regions, which are indexed by $n \in \{1, 2, \cdots, 8\}$.

belonging to one region), denoted as $\mathbb{R}^2_{(1)}, \mathbb{R}^2_{(2)}, \cdots, \mathbb{R}^2_{(8)}$, as illustrated in Fig. 3. Note that this partition ensures that $\{\Sigma \cap \mathbb{R}^2_{(n)}\}$ are independent. In addition, the eight regions can be classified into two groups: regions indexed by $\{1, 3, 5, 7\}$ and regions indexed by $\{2, 4, 6, 8\}$. The geometric characteristics of all regions in the same group are the same, and the characteristics of the two groups are different. Let

$$\begin{aligned} R_n \triangleq \arg\max \quad & r \\ \mathbf{s.t.} \quad & r \in \left\{ \sqrt{s}(n + \frac{1}{2}) : n = 0, 1, \cdots \right\}, \\ & \mathcal{B}(r) \cap \Sigma \cap \mathbb{R}^2_{(n)} = \emptyset. \end{aligned}$$

Then, $\mathcal{B}(R_n) \cap \mathbb{R}^2_{(n)}$ is the blockage-free region in $\mathbb{R}^2_{(n)}$ with the largest radius. Notice that due to the independence of $\{\Sigma \cap \mathbb{R}^2_{(n)}\}$, $\{R_n\}$ are independent and so are $\{\mathcal{B}(R_n) \cap \mathbb{R}^2_{(n)}\}$. One can see that, the combined region $\bigcup_n \left(\mathcal{B}(R_n) \cap \mathbb{R}^2_{(n)}\right)$ has more geometric degrees-of-freedoms in approaching $\mathcal{F}$ than $\mathcal{B}(R)$, yielding a tighter inner bound for $\mathcal{F}$. That is, we have

$$\mathcal{B}(R) \subseteq \cup_n \left(\mathcal{B}(R_n) \cap \mathbb{R}^2_{(n)}\right) \subseteq \mathcal{F}. \tag{17}$$

Then replacing $\mathcal{F}$ with $\bigcup_n \left(\mathcal{B}(R_n) \cap \mathbb{R}^2_{(n)}\right)$ in the definition of the connectivity probability given in (1) leads to a tighter lower bound than that in (8):

$$\begin{aligned} p_c &\geq \Pr\left\{ \cup_n \left(\mathcal{B}(R_n) \cap \mathbb{R}^2_{(n)}\right) \cap \mathcal{B}(r_b) \cap \Pi \neq \emptyset \right\} \\ &= 1 - \Pr\left\{ \cup_n \left(\mathcal{B}(R_n) \cap \mathbb{R}^2_{(n)}\right) \cap \mathcal{B}(r_b) \cap \Pi = \emptyset \right\} \end{aligned}$$

$$\stackrel{(a)}{=} 1-\prod_{n=1}^{8}\Pr\Big\{\mathcal{B}(R_n)\cap\mathcal{B}(r_b)\cap\mathbb{R}^2_{(n)}\cap\Pi=\emptyset\Big\}$$
$$=1-\prod_{n=1}^{8}\Big(1-\tilde{p}_c^{(n)}\Big), \tag{18}$$

where

$$\tilde{p}_c^{(n)}=\Pr\Big\{\mathcal{B}(\min(R_n,r_b))\cap\mathbb{R}^2_{(n)}\cap\Pi\neq\emptyset\Big\} \tag{19}$$

represents the connectivity probability in region $\mathbb{R}^2_{(n)}$ and (a) is due to the independence of $\{\mathcal{B}(R_n)\cap\mathbb{R}^2_{(n)}\cap\Pi\}$.

Using (18), a closed-form expression for the tighter lower bound on p_c can be derived following a similar procedure as in the preceding sub-section. To this end, one can observe the similarity in the expressions for $\tilde{p}_c^{(n)}$ in (19) and the lower bound on p_c in (8). Then adopting a similar procedure as for deriving Theorem 1 results in Lemma 3 in the sequel. The details are omitted for brevity.

Lemma 3. The connectivity probabilities $\{\tilde{p}_c^{(n)}\}$ defined in (19) can be bounded as follows.

– For $n=1$, 3, 5, and 7, $\tilde{p}_c^{(n)}\geq q^{(n)}$ where

$$q^{(n)}=\left(1-\exp\Big(-s\lambda_c\Big\lfloor\frac{r_b}{\sqrt{s}}-\frac{1}{2}\Big\rfloor^+\Big)\right)\bar{p}_b^{\lceil\frac{r_b}{\sqrt{s}}-\frac{1}{2}\rceil^+}$$
$$+\sum_{\ell=0}^{\lfloor\frac{r_b}{\sqrt{s}}-\frac{1}{2}\rfloor^+}p_b\Big(1-e^{-s\lambda_c\ell}\Big)\bar{p}_b^{\ell}. \tag{20}$$

– For $n=2$, 4, 6, and 8, $\tilde{p}_c^{(n)}\geq q^{(n)}$ where

$$q^{(n)}=\left(1-\exp\Big(-\frac{1}{4}\pi s\lambda_c\Big(\Big\lfloor\frac{r_b}{\sqrt{s}}-\frac{1}{2}\Big\rfloor^+\Big)^2\Big)\right)\bar{p}_b^{\left(\lceil\frac{r_b}{\sqrt{s}}-\frac{1}{2}\rceil^+\right)^2}$$
$$+\sum_{\ell=0}^{\lfloor\frac{r_b}{\sqrt{s}}-\frac{1}{2}\rfloor^+}\Big(1-e^{-\frac{1}{4}\pi s\lambda_c\ell^2}\Big)\bar{p}_b^{\ell^2}\Big(1-\bar{p}_b^{2\ell+1}\Big). \tag{21}$$

Note that in (20) for $n=1,3,5,7$, $s\Big\lfloor\frac{r_b}{\sqrt{s}}-\frac{1}{2}\Big\rfloor^+$ is the area of $\mathcal{B}(r_b)\cap\mathbb{R}^2_{(n)}$ and $s\ell$ is a lower bound on the area of $\mathcal{B}(r_\ell)\cap\mathbb{R}^2_{(n)}$; in (21) for $n=2,4,6,8$, $\frac{1}{4}\pi s\Big(\Big\lfloor\frac{r_b}{\sqrt{s}}-\frac{1}{2}\Big\rfloor^+\Big)^2$ is the area of $\mathcal{B}(r_b)\cap\mathbb{R}^2_{(n)}$ and $\frac{1}{4}\pi s\ell^2$ is an lower bound on the area of $\mathcal{B}(r_\ell)\cap\mathbb{R}^2_{(n)}$.

Substituting Lemma 3 into (18) yields the following main result of this sub-section, which improves the result in Theorem 1.

Theorem 3. An alternative lower bound on the network-connectivity probability for the single-tier network is

$$p_c \geq 1 - \prod_{n=1}^{8} \left(1 - q^{(n)}\right), \tag{22}$$

where $\{q^{(n)}\}$ are given in Lemma 3.

Consider the case where $\{\tilde{p}_c^{(n)}\}$ are small. Then it follows from (18) and Lemma 3 that

$$p_c \geq \sum_{n=1}^{8} \tilde{p}_c^{(n)} \geq \sum_{n=1}^{8} q^{(n)}. \tag{23}$$

The summation reflects the improvement on the tightness of the lower bound on p_c with respect to that in Theorem 1. That is, in the case of small $\{\tilde{p}_c^{(n)}\}$, it can be seen more clearly that the result in Theorem 3 improves that in Theorem 1.

Consider the network with high site density ($\lambda_s \to \infty$). The areas of the regions $\mathbb{R}^2_{(1)}, \mathbb{R}^2_{(3)}, \mathbb{R}^2_{(5)}$, and $\mathbb{R}^2_{(7)}$ are close to zero when the site density λ_s is sufficiently large (i.e., site area s is sufficiently small), which can be easily seen from Fig. 3, and thus can be ignored for ease of analysis. Following a similar procedure presented in the preceding sub-section, an asymptotic lower bound on the connectivity probability is derived as follows.

Theorem 4. For the case of high site density ($\lambda_s \to \infty$), an alternative lower bound on the connectivity probability for the single-tier network is

$$p_c \geq 1 - (1 - \tilde{p}_c)^4, \tag{24}$$

where

$$\tilde{p}_c = \frac{1}{1 - \frac{\lambda_s}{4\lambda_c} \ln \bar{p}_b} \left(1 - \bar{p}_b^{\frac{1}{4}\lambda_s \pi r_b^2} e^{-\frac{1}{4}\pi\lambda_c r_b^2}\right) + \frac{1}{1 - \frac{4\lambda_c}{\lambda_s \ln \bar{p}_b}} \left(1 - e^{-\frac{\pi}{4}\frac{\lambda_c}{\lambda_s}}\right). \tag{25}$$

Similarly, the result in Theorem 4 improves that in Theorem 2. For the case where $\tilde{p}_c$ is small, it follows from Theorem 4 that $p_c \geq 4\tilde{p}_c$, where the factor 4 arises from the number of the main regions $\mathbb{R}^2_{(2)}, \mathbb{R}^2_{(4)}, \mathbb{R}^2_{(6)}, \mathbb{R}^2_{(8)}$ in the partition of the plane (see Fig. 3). The factor 4 reflects the tightening of the lower bound on p_c due to the partition approach, omitting the relatively small reduction on $\tilde{p}_c$ due to the approach. In general, increasing the number of regions in the partition leads to a more accurate approximation of the blockage-free region (see Fig. 2(a)) and hence an increasingly tighter lower bound on p_c.

C. Randomly Located Typical User

The preceding analysis assumes a typical outdoor user at the origin for ease of notation and expression. Extending the results to the general case of a randomly located user is straightforward. To incorporate the effect due to the random offset of the typical user from the origin in a traceable manner, r in the upper bound of Lemma 1 is replaced with $r+\frac{1}{2}\sqrt{s}$, while r in the lower bound of Lemma 1 is replaced with $r-\frac{1}{2}\sqrt{2s}$. In other words, for the case of a randomly located user, the result in Lemma 1 can be modified as follows:

$$\left(2\left\lceil\frac{r}{\sqrt{2s}}-1\right\rceil^{+}+1\right)^{2}\leq N(r)\leq\left(2\left\lceil\frac{r}{\sqrt{s}}\right\rceil^{+}+1\right)^{2}. \tag{26}$$

Then, it is straightforward for modifying other analytical results accordingly, without changing the key insight.

IV. Connectivity of Heterogeneous Networks

In the preceding section, the connectivity probabilities are analyzed for the single-tier mmWave network. Noting that the HetNet provides a promising approach to satisfy the rapid traffic growth by deploying short range small BSs (e.g., pico BSs) together with traditional macro BSs. The results are extended in this section to the K-tier mmWave HetNet. Specifically, we extend the bounds on the connectivity probability based on the approach of inner bounding the blockage-free region using a disk. The resulting bounds can be also tightened following the same approach as in the last section. The procedure is straightforward and the details are omitted for brevity.

It is challenging to give an exact result for $\widehat{p}_c$ due to the spatial correlation of $\{\mathcal{F}^{(k)}\}$. For analytical tractability, a lower bound on $\widehat{p}_c$ is given by selecting the largest value of the network connectivity probabilities of the K tiers. Mathematically, the connectivity probability for the K-tier HetNet as defined in (2) is lower bounded as follows

$$\begin{aligned}\widehat{p}_c&=\Pr\left\{\bigcup_{k=1}^{K}\left(\mathcal{F}^{(k)}\cap\mathcal{B}(r_b^{(k)})\cap\Pi^{(k)}\right)\neq\emptyset\right\}\\&\geq\max_{k\in\{1,\cdots,K\}}p_c^{(k)},\end{aligned} \tag{27}$$

where $p_c^{(k)}\triangleq\Pr\left\{\mathcal{F}^{(k)}\cap\mathcal{B}(r_b^{(k)})\cap\Pi^{(k)}\neq\emptyset\right\}$ represents the connectivity probability for the kth-tier network.

The per-tier connectivity probabilities $\{p_c^{(k)}\}$ can be bounded by modifying the lower bound on the single-tier counterpart in Theorem 1. Specifically, the modification involves replacing the blockage-occupancy probability p_b with $(1-\prod_{\ell=1}^{k}\bar{p}_b^{(\ell)})$ since the signals transmitted by a BS

in the kth tier network can be blocked by buildings of heights $h^{(1)}, \cdots, h^{(k)}$, as illustrated in Section II. This yields the following corollary of Theorem 1.

Corollary 1 (Per-tier Connectivity Probability for the K-tier HetNet)**.** The connectivity probability for the kth tier network can be lower bounded as $p_c^{(k)} \geq \eta^{(k)}$, where

$$\eta^{(k)} = \left(1 - e^{-\pi\lambda_c^{(k)}\left(r_b^{(k)}\right)^2}\right) q_k^{N^+\left(r_b^{(k)}\right)-1} + \sum_{n=0}^{\left\lfloor \frac{r_b^{(k)}}{\sqrt{s}} - \frac{1}{2} \right\rfloor^+} \left(1 - e^{-\pi s \lambda_c^{(k)}(n+\frac{1}{2})^2}\right) q_k^{4(n+\frac{1}{2})^2-1} \left(1 - q_k^{8(n+1)}\right), \tag{28}$$

$q_k = \prod_{\ell=1}^{k} \bar{p}_b^{(\ell)}$ and $N^+(r_b^{(k)})$ is given in (4).

It is worth mentioning that q_k can be rewritten as $\left(1 - \sum_{\ell=1}^{k} p_b^{(\ell)}\right)$ when $\{p_b^{(k)}\}$ are small, giving a simple form. Substituting the result in Corollary 1 into (27) leads to the first main result of this section.

Theorem 5 (Connectivity Probability for the K-tier HetNet)**.** The connectivity probability for the K-tier HetNet can be lower bounded as

$$\widehat{p}_c \geq \max_{k \in \{1, \cdots, K\}} \eta^{(k)}, \tag{29}$$

where $\eta^{(k)}$ is defined in Corollary 1.

Next, consider the case with a high site density ($\lambda_s \to \infty$) as before. By modifying the result in Corollary 1 in the same way as for obtaining Theorem 2, the connectivity probability for the kth tier network is as shown in Corollary 2.

Corollary 2 (Per-tier Connectivity Probability for the K-tier HetNet with Dense Sites)**.** When the site density is high $\lambda_s \to \infty$, the connectivity probability for the kth tier network is bounded as $p_c^{(k)} \geq \eta^{(k)}$ with

$$\eta^{(k)} = \frac{1}{1 + \frac{\lambda_s}{\lambda_c^{(k)}} \ln \frac{1}{q_k}} \left(1 - e^{-\pi\lambda_c^{(k)}\left(r_b^{(k)}\right)^2\left(1 + \frac{\lambda_s}{\lambda_c^{(k)}} \ln \frac{1}{q_k}\right)}\right) + \frac{1}{1 + \frac{\lambda_c^{(k)}}{\lambda_s \ln \frac{1}{q_k}}} \left(1 - e^{-\pi \frac{\lambda_c^{(k)}}{\lambda_s}}\right), \tag{30}$$

and q_k follows that in Corollary 1.

Corollary 2 gives a closed-form lower bound on the connectivity probability for the kth tier network with dense sites. By Theorem 5 and Corollary 2, the connectivity probability for the K-tier HetNet with dense sites is obtained as shown below.

Theorem 6 (Connectivity Probability for the K-tier HetNet with Dense Sites)**.** For the case of dense sites ($\lambda_s \to \infty$), the connectivity probability for the K-tier HetNet can be lower bounded as

$$\widehat{p}_c \geq \max_{k\in\{1,\cdots,K\}} \eta^{(k)}, \tag{31}$$

where $\eta^{(k)}$ is given in Corollary 2.

The lower bound can be tightened using the same approach as in the preceding section. The results are summarized in the following theorem.

Theorem 7. An alternative lower bound on the connectivity probability for the K-tier HetNet is

$$\widehat{p}_c \geq \max_{k\in\{1,\cdots,K\}} \left\{1 - \prod_{n=1}^{8} \left(1-\eta^{(k,n)}\right)\right\}, \tag{32}$$

where $\{\eta^{(k,n)}\}$ are stated as follows.

– For $n = 1$, 3, 5, and 7:

$$\eta^{(k,n)} = \left(1 - e^{-s\lambda_c^{(k)}\left\lfloor \frac{r_b^{(k)}}{\sqrt{s}}-\frac{1}{2}\right\rfloor^+}\right) q_k^{\left\lceil \frac{r_b^{(k)}}{\sqrt{s}}-\frac{1}{2}\right\rceil^+} + \sum_{\ell=0}^{\left\lfloor \frac{r_b^{(k)}}{\sqrt{s}}-\frac{1}{2}\right\rfloor^+} \left(1-e^{-s\lambda_c^{(k)}\ell}\right)\bar{q}_k q_k^{\ell}. \tag{33}$$

– For $n = 2$, 4, 6, and 8:

$$\eta^{(k,n)} = \left(1 - e^{-\frac{\pi s}{4}\lambda_c^{(k)}\left(\left\lfloor \frac{r_b^{(k)}}{\sqrt{s}}-\frac{1}{2}\right\rfloor^+\right)^2}\right) q_k^{\left(\left\lceil \frac{r_b^{(k)}}{\sqrt{s}}-\frac{1}{2}\right\rceil^+\right)^2} + \sum_{\ell=0}^{\left\lfloor \frac{r_b^{(k)}}{\sqrt{s}}-\frac{1}{2}\right\rfloor^+} \left(1-e^{-\frac{\pi s}{4}\lambda_c^{(k)}\ell^2}\right) q_k^{\ell^2}\left(1-q_k^{2\ell+1}\right). \tag{34}$$

Here, $q_k = \prod_{\ell=1}^{k} \bar{p}_b^{(\ell)}$.

An approximation of $\widehat{p}_c$ can be obtained if the spatial correlation of $\{\mathcal{F}^{(k)}\}$ is ignored. Mathematically, the approximation of $\widehat{p}_c$ is given as follows:

$$\begin{aligned}
\widehat{p}_c &= 1 - \Pr\left\{\bigcup_{k=1}^{K}\left(\mathcal{F}^{(k)} \cap \mathcal{B}(r_b^{(k)}) \cap \Pi^{(k)}\right) = \emptyset\right\} \\
&= 1 - \Pr\left\{\mathcal{F}^{(1)} \cap \mathcal{B}(r_b^{(1)}) \cap \Pi^{(1)} = \emptyset, \cdots, \mathcal{F}^{(K)} \cap \mathcal{B}(r_b^{(K)}) \cap \Pi^{(K)} = \emptyset\right\} \\
&\approx 1 - \prod_{k=1}^{K} \Pr\left\{\mathcal{F}^{(k)} \cap \mathcal{B}(r_b^{(k)}) \cap \Pi^{(k)} = \emptyset\right\}
\end{aligned}$$

$$= 1 - \prod_{k=1}^{K} \left(1 - p_c^{(k)}\right). \tag{35}$$

Remark 1 (Gain of Multiple Tiers)**.** If the connectivity probability for each tier of the K-tier HetNet is small, namely that $p_c^{(k)} \to 0$ for all $k = 1, \cdots, K$, it follows from (35) that the network connectivity probability for the K-tier HetNet can be further approximated as $\widehat{p}_c \approx \sum_{k=1}^{K} p_c^{(k)}$. This quantifies the gain of multiple tiers of a HetNet that adding one more tier of BSs can linearly increase the connectivity probability.

Combining the result in Corollary 1 and (35) gives the following result.

Theorem 8 (Connectivity Probability for the K-tier HetNet)**.** The connectivity probability for the K-tier HetNet can be approximately lower bounded by

$$\widehat{p}_c > 1 - \prod_{k=1}^{K} \left(1 - \eta^{(k)}\right), \tag{36}$$

where $\eta^{(k)}$ is defined in Corollary 1.

The lower bounder in Theorem 8 can be further tightened using the same approach as in the preceding section, giving

$$\widehat{p}_c > 1 - \prod_{k=1}^{K} \left(\prod_{n=1}^{8} \left(1 - \eta^{(k,n)}\right) \right), \tag{37}$$

where $\{\eta^{(k,n)}\}$ are given in Theorem 7.

V. Simulation Results

In this section, both the Monte Carlo simulation and analytical results for characterizing the network connectivity based on the proposed random lattice building modeling are presented and compared to illustrate how the blockage effect impacts the network performance in an urban scenario. The single-tier network is considered first and followed by the K-tier HetNet. The results are obtained based on the following parameter setting unless stated otherwise. In the single-tier network, assume the coverage range of a BS r_b is 150 meters (m). The BS density is $\lambda_c = 6 \times 10^{-5}$ per square meter ($1/\mathrm{m}^2$) with the site area $s = 30\ \mathrm{m}^2$. The building occupation probability is $p_b = 0.3$. For the K-tier HetNet, we assume the number of tiers $K = 3$. The corresponding BS coverage ranges of tier 1, 2, 3 are specified as $\{r_b^{(1)}, r_b^{(2)}, r_b^{(3)}\} = \{150, 90, 50\}$ m, respectively. The density of BSs in each tier increases, given by $\lambda_c^{(1)} = 4 \times 10^{-5}\ 1/\mathrm{m}^2$, $\lambda_c^{(2)} = 5\lambda_c^{(1)}$, and $\lambda_c^{(3)} = 10\lambda_c^{(1)}$ and the building occupation probabilities are listed as $\{p_b^{(0)}, p_b^{(1)}, p_b^{(2)}, p_b^{(3)}\} = \{0.4, 0.1, 0.2, 0.3\}$.

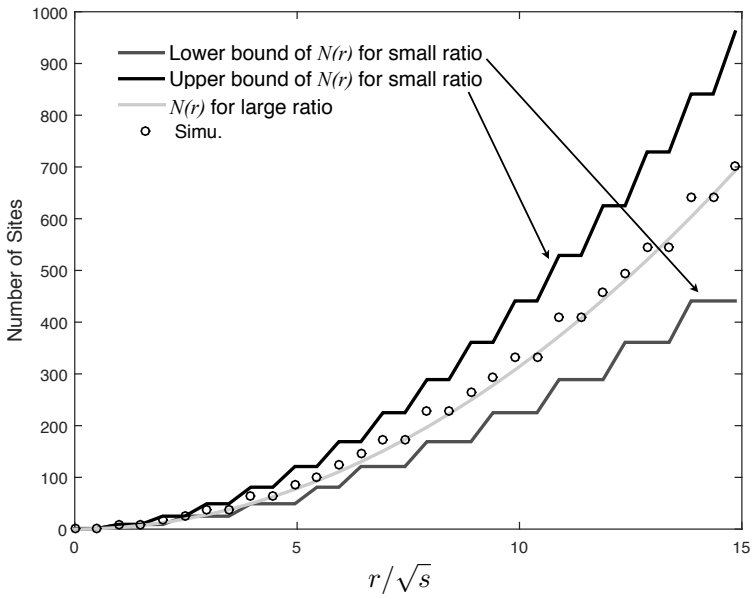

Figure 4: Number of sites (fully and partially) covered by a disk with radius r versus the ratio $\frac{r}{\sqrt{s}}$.

Both simulation and analytical results are plotted and compared based on the proposed blockage-free region partition approaches, namely MBFC region approach and *multiple sub-regions* (multi-region) partition approach. In each figure, we consider the following two setups for numerically plotting the analytical curves: *i*) the analytical result with a normal site density (i.e., normal site area), *ii*) the analytical result with a high site density (i.e., small site area). For the markers in the figures, the Monte Carlo simulation results are represented using the circles: use red circles stand for the simulation results of the real network scenario and black circles stand for the simulation results of the lower bounds, while the analytical results of two aforementioned approaches are plotted via the short-dashed line and solid line, respectively.

First, the result in Lemma 1 is validated in Fig. 4 by plotting the number of (fully and partially) covered sites within $\mathcal{B}(r)$, say $N(r)$, against the ratio $\frac{r}{\sqrt{s}}$. It can be observed that the Monte Carlo simulation results (marked via black circles) are tightly bounded by the analytical results given in (4) when the ratio $\frac{r}{\sqrt{s}}$ is small and closely match with the light grey curve drawn using (5) in the high ratio range, confirming the accuracy of Lemma 1.

In Fig. 5, the connectivity probability of the single-tier network is plotted versus the BS density for different region partition approaches. Firstly, the analytical results calculated using Theorem 1 match the Monte Carlo simulation results (black circles) closely. It can be observed from the figure that the connectivity probability p_c increases as the BS density λ_c increases, namely, the network connectivity will benefit from a denser BS deployment since deploying more BSs leads to a larger service coverage and thus fewer coverage holes. Another observation

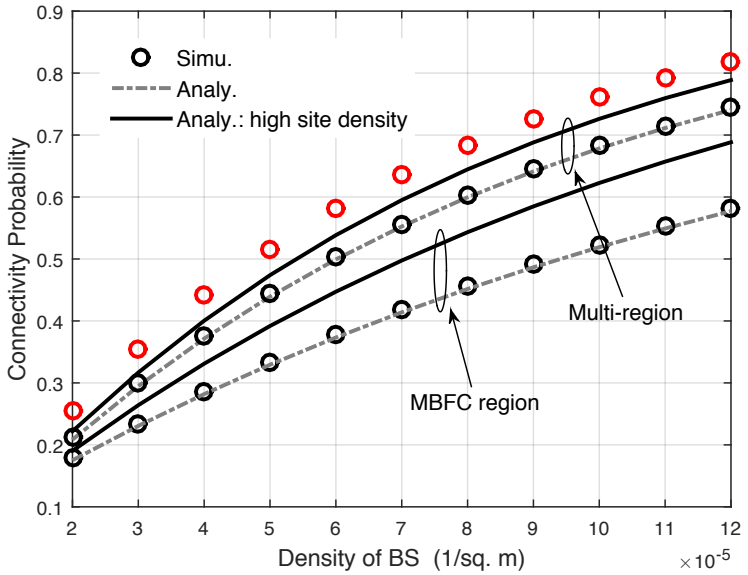

Figure 5: Connectivity probability versus BS density for different blockage-free region partition approaches, MBFC region and multi-region, in the single-tier network.

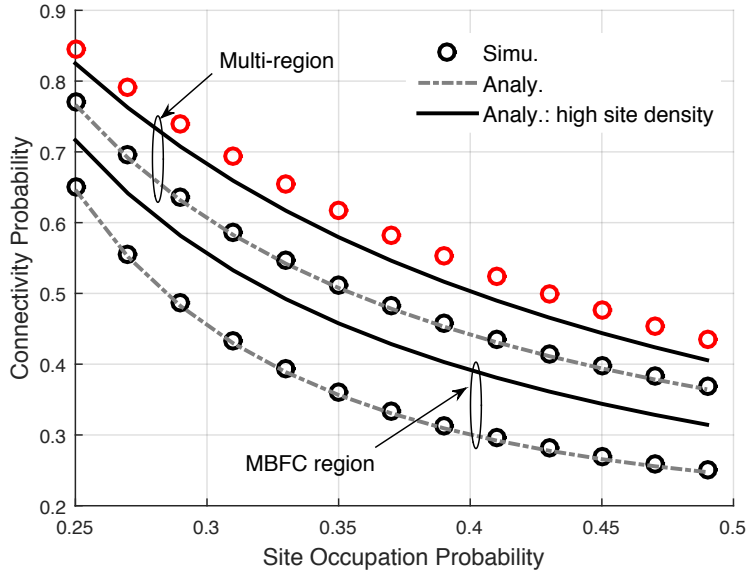

Figure 6: Connectivity probability versus site occupation probability for different blockage-free region partition approaches, MBFC region and multi-region, in the single-tier network.

is that the analytical result for the network with a high site density ($\lambda_s \to \infty$) given in Theorem 2 performs the better lower bounds compared with that of the network with a normal site area. Moreover, the bounds have been tightened by partitioning the network into eight independent regions, which gives a small gap with respect to the simulation result of the real scenario marked by red circles. The gap seems to be an acceptable compromise between accuracy of characterizing the connectivity probability and analytical tractability.

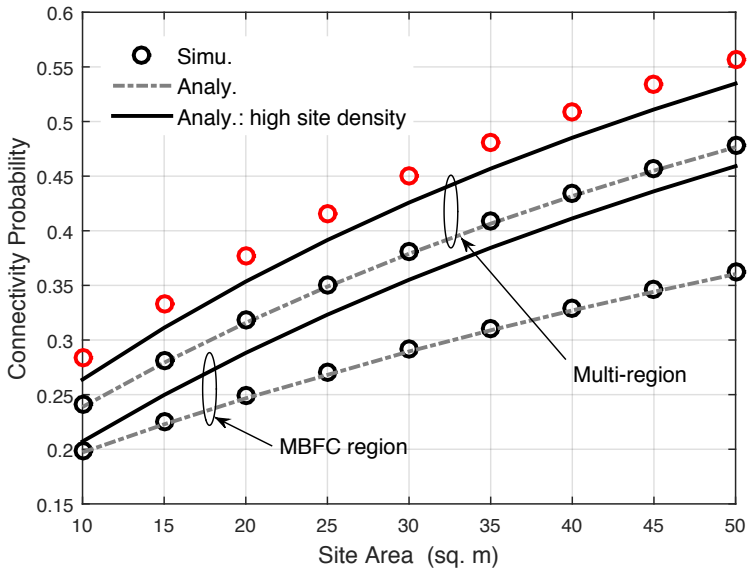

Figure 7: Connectivity probability versus site area for different blockage-free region partition approaches, MBFC region and multi-region, in the single-tier network.

Fig. 6 shows the curves of p_c in the single-tier network versus the site occupation probability p_b. It is found that increasing the site occupation probability weakens the network connectivity and p_c degrades significantly when p_b is relatively small $(0.25 - 0.35)$ and converges to some value if p_b becomes quite larger. This is because densifying the buildings intercepts more LoS links of mmWave signals and enlarges the communication coverage holes, resulting in a lower connectivity probability.

Next, the effect of the site density, i.e., site area s, on the single-tier network connectivity is investigated in Fig. 7. Obviously, increasing the site area s, i.e., decreasing the site density $\lambda_s = \frac{1}{s}$, will dramatically improve the network connectivity. It is easy to understand due to the fact that, given the site occupation probability p_b, a smaller site density yields fewer opportunities for buildings occupying the sites nearby the typical user, which is equivalent to enlarge the blockage-free region for BSs to be located thus provide better connectivity. Another observation is that the analytical curves for small s are closely matched with the analytical curves as well as simulation results when the site area goes to sufficiently small, which verifies the correctness of our analytical results under the high site density assumption ($\lambda_s \to \infty$).

Consider the connectivity probability in the K-tier HetNet where $K = 3$. The curves of connectivity probability $\widehat{p}_c$ are depicted against the number of tiers in Fig. 8. The approximation of connectivity probability by neglecting correlations of multiple tiers is also plotted for comparison, marked as long-dashed line. As stated in the figure, $\widehat{p}_c$ is observed to grow approximately linearly

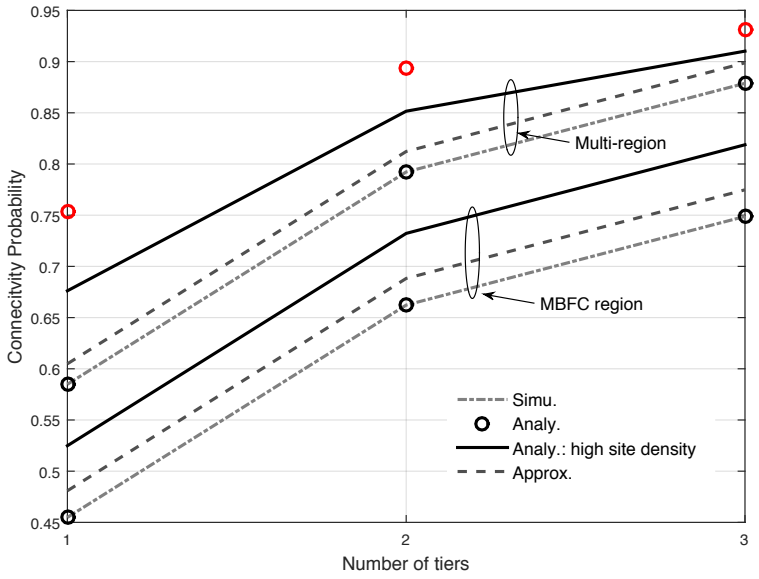

Figure 8: Connectivity probability versus number of tiers for different blockage-free region partition approaches, MBFC region and multi-region, in a K-tier HetNet.

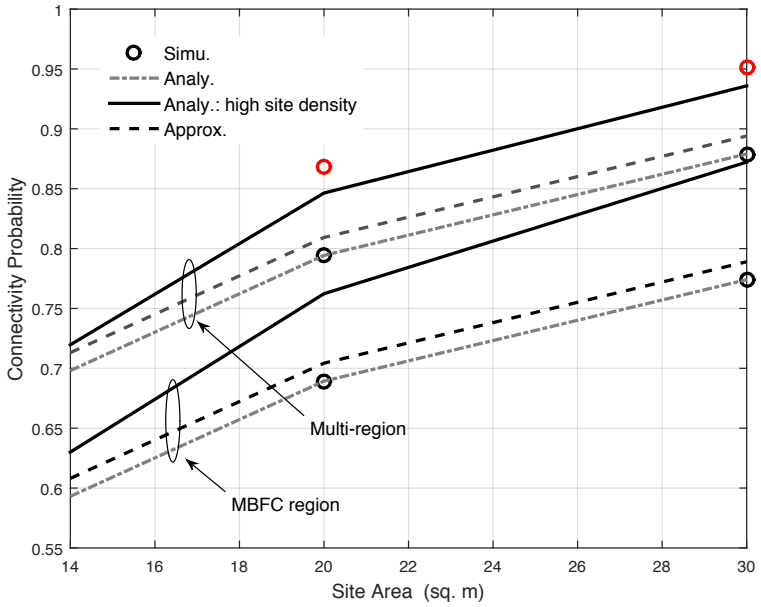

Figure 9: Connectivity probability versus site area for different blockage-free region partition approaches, MBFC region and multi-region, in a K-tier HetNet where $K = 3$.

with the number of tiers and saturate when K is large, agreeing the discussion in Remark 1. The bounds are remarkably tightened by partitioning the network into multi-region. Fig. 9 displays the curves of the network connectivity versus the site area, or site density, in the 3-tier HetNet. The connectivity probability grows when the site area s increases. Moreover, the analytical results based on the high site density assumption asymptotically approach to the simulation results.

VI. Conclusion Remarks

Recently, researchers have studied the performance of large-scale mmWave radio access networks in the presence of the blockage effect using stochastic geometry models for blockage objects (e.g., buildings) and network nodes. Typically, buildings are modeled using the Boolean model and streets as a Poisson-line process but such models are unsuitable for Manhattan-type cities. To address this issue, we have made the first attempt that model building as a random lattice and apply this model to investigate the connectivity performance of Poisson distributed BSs in mmWave networks. Our study has yielded useful closed-form relations between the parameters of the building process and the BS process, providing useful guidelines for practical mmWave network deployment. The work opens up many directions for future extensions. In particular, accounting for the effect of interference and integrating multi-antenna techniques pose interesting research opportunities.

Appendix

A. *Proof of Lemma 2*

Characterizing the PMF of the random variable R is equivalent to derive the area distribution of MBFC region. Denote the area measure by $\mathcal{A}(\cdot)$. Note that $\mathcal{A}(\mathcal{B}(R))$ represents the area of $\mathcal{B}(R)$, we have the following equivalent relation: $\Pr\left(R=r_n\right)=\Pr\left(\mathcal{A}(\mathcal{B}(R))=\pi r_n^2\right)$. For clear explanation, let $\mathcal{E}(r)$ be the event that there is no occupied site within $\mathcal{B}(r)$ and let $\bar{\mathcal{E}}(r)$ denote the complement event. Then, using the total probability rule gives the following result.

$$\begin{aligned}
&\Pr\left(\mathcal{A}(\mathcal{B}(R))=\pi r_n^2\right)\\
=&\Pr\left(\mathcal{E}(r_n),\bar{\mathcal{E}}(r_{n+1})|\mathcal{E}(0)\right)\\
=&\Pr\left(\mathcal{E}(r_n)|\mathcal{E}(0)\right)-\Pr\left(\mathcal{E}(r_{n+1})|\mathcal{E}(0)\right)\\
=&\Pr\left(\mathcal{E}(r_n),\mathcal{E}(0)\right)-\Pr\left(\mathcal{E}(r_{n+1}),\mathcal{E}(0)\right),
\end{aligned}\tag{38}$$

where the last step is obtained due to the condition that $\Pr\left(\mathcal{E}(0)\right)=1$. Combining the facts that the probability of each site is not occupied is $\bar{p}_b$ and the occupancy of each site is independent gives the following result:

$$\Pr\left(R=r_n\right)=\bar{p}_b^{N(r_n)-1}-\bar{p}_b^{N(r_{n+1})-1},\qquad n=0,1,2,\cdots.\tag{39}$$

It is easy to calculate the number of (empty) sites within MBFC region $\mathcal{B}(r_n)$ is $(2(n+\frac{1}{2}))^2$. Therefore, substituting $N(r_n)=(2(n+\frac{1}{2}))^2$ into (39) yields the final result.

REFERENCES

[1] T. Rappaport, S. Sun, R. Mayzus, H. Zhao, Y. Azar, K. Wang, G. Wong, J. Schulz, M. Samimi, and F. Gutierrez, "Millimeter wave mobile communications for 5G cellular: It will work!," *IEEE Access*, vol. 1, pp. 335–349, 2013.

[2] J. Andrews, S. Buzzi, W. Choi, S. Hanly, A. Lozano, A. Soong, and J. Zhang, "What will 5G be?," *IEEE J. of Sel. Areas in Commun.*, vol. 32, pp. 1065–1082, Jun. 2014.

[3] C. Anderson and T. Rappaport, "In-building wideband partition loss measurements at 2.5 and 60 GHz," *IEEE Trans. Wireless Commun.*, vol. 3, pp. 922–928, May. 2004.

[4] A. Alejos, M. Sánchez, and I. Cuiñas, "Measurement and analysis of propagation mechanisms at 40 GHz: Viability of site shielding forced by obstacles," *IEEE Trans. Veh. Technol.*, vol. 57, pp. 3369–3380, Nov. 2008.

[5] A. Goldsmith, *Wireless communications*. Cambridge university press, 2005.

[6] J. Andrews, T. Bai, M. Kulkarni, A. Alkhateeb, A. Gupta, and R. Heath, Jr, "Modeling and analyzing millimeter wave cellular systems," *(online) Available: https://arxiv.org/abs/1605.04283*, May. 2016.

[7] K. Schaubach, N. Davis IV, and T. Rappaport, "A ray tracing method for predicting path loss and delay spread in microcellular environments," in *Proc. of IEEE VTC*, pp. 932–935, May. 1992.

[8] K. Rizk, J. Wagen, and F. Gardiol, "Two-dimensional ray-tracing modeling for propagation prediction in microcellular environments," *IEEE Trans. Veh. Technol.*, vol. 46, pp. 508–518, May 1997.

[9] G. T. 36.873, "Echnical specification group radio access network; study on 3d channel model for lte (release 12)," Sep. 2014.

[10] M. Akdeniz, Y. Liu, M. Samimi, S. Sun, S. Rangan, T. Rappaport, and E. Erkip, "Millimeter wave channel modeling and cellular capacity evaluation," *IEEE J. Sel. Areas Commun.*, vol. 32, pp. 1164–1179, Jun. 2014.

[11] S. Sun, T. Thomas, T. Rappaport, H. Nguyen, I. Kovacs, and I. Rodrigue, "Path loss, shadow fading, and line-of-sight probability models for 5G urban macro-cellular scenariosc," *Proc. IEEE GLOBECOM Workshops*, Dec. 2015.

[12] "5G channel model for bands up to 100 GHz (white paper)," in *Available: http://www.5gworkshops.com/5GCM.html*, Dec. 2015.

[13] T. Bai, R. Vaze, and R. Heath, Jr, "Analysis of blockage effects on urban cellular networks," *IEEE Trans. Wireless Commun.*, vol. 13, pp. 5070–5083, Sep. 2014.

[14] F. Baccelli and X. Zhang, "A correlated shadowing model for urban wireless networks," in *Proc. of IEEE INFOCOM*, pp. 801–809, Apr. 2015.

[15] M. Haenggi, J. Andrews, F. Baccelli, O. Dousse, and M. Franceschetti, "Stochastic geometry and random graphs for the analysis and design of wireless networks," *IEEE J. of Sel. Areas in Commun.*, vol. 27, pp. 1029–1046, Sep. 2009.

[16] J. Andrews, F. Baccelli, and R. Ganti, "A tractable approach to coverage and rate in cellular networks," *IEEE Trans. Commun.*, vol. 59, pp. 3122–3134, Nov. 2011.

[17] R. Ganti and M. Haenggi, "Interference and outage in clustered wireless ad hoc networks," *IEEE Trans. Info. Theory*, vol. 9, pp. 4067–4086, Sep. 2009.

[18] A. Gupta, J. Andrews, and R. Heath, Jr, "Macro diversity in cellular networks with random blockages," *(online) Available: https://arxiv.org/abs/1701.02044*, Jan. 2017.

[19] T. Bai and R. Heath, Jr, "Coverage in dense millimeter wave cellular networks," in *Proc. of ASILOMAR*, pp. 2062–2066, Nov. 2013.

[20] S. Singh, M. Kulkarni, A. Ghosh, and J. Andrews, "Tractable model for rate in self-backhauled millimeter wave cellular networks," *IEEE J. of Sel. Areas in Commun.*, vol. 33, pp. 2196–2211, Oct. 2015.

[21] G. Franceschetti, S. Marano, and F. Palmieri, "Propagation without wave equation toward an urban area model," *IEEE Trans. Antennas Propag.*, vol. 47, pp. 1393–1404, Sep. 1999.

[22] S. Marano, F. Palmieri, and G. Franceschetti, "Statistical characterization of ray propagation in a random lattice," *J. Opt. Soc. Amer. A*, vol. 16, pp. 2459–2464, Oct. 1999.

[23] S. Marano and M. Franceschetti, "Ray propagation in a random lattice: a maximum entropy, anomalous diffusion process," *IEEE Trans. Antennas Propag.*, vol. 53, pp. 1888–1896, Jun. 2005.

[24] G. Mao and B. Anderson, "Towards a better understanding of large-scale network models," *IEEE/ACM Trans. on Networking*, vol. 20, no. 2, pp. 408–421, 2012.

[25] F. Xue and P. Kumar, "The number of neighbors needed for connectivity of wireless networks," *Wireless networks*, vol. 10, no. 2, pp. 169–181, 2004.

[26] P. Gupta and P. Kumar, "Critical power for asymptotic connectivity in wireless networks," in *Stochastic analysis, control, optimization and applications*, pp. 547–566, Springer, 1999.

[27] P. Gupta and P. Kumar, "The capacity of wireless networks," *IEEE Trans. Info. Theory*, vol. 46, pp. 388–404, Mar. 2000.

[28] O. Dousse, F. Baccelli, and P. Thiran, "Impact of interferences on connectivity in ad hoc networks," *IEEE/ACM Trans. on Networking*, vol. 13, no. 2, pp. 425–436, 2005.

[29] G. Mao and B. Anderson, "Connectivity of large wireless networks under a general connection model," *IEEE Trans. Info. Theory*, vol. 59, pp. 1761–1772, Mar. 2013.

[30] S. Dasgupta, G. Mao, and B. Anderson, "A new measure of wireless network connectivity," *IEEE Trans. on Mobile Computing*, vol. 14, pp. 1765–1779, Sep. 2015.